Available online at www.sciencedirect.com
ScienceDirect
Journal of Contaminant Hydrology 90 (2007) 58–80
JOURNAL OF Contaminant Hydrology
www.elsevier.com/locate/jconhyd

Modelling the long-term performance of zero-valent iron using a spatio-temporal approach for iron aging

Irina Kouznetsova [a], Peter Bayer [a], Markus Ebert [b], Michael Finkel [a,*]

[a] *Center for Applied Geoscience, University of Tuebingen, Sigwartstrasse 10, 72076 Tuebingen, Germany*
[b] *Institute of Geosciences, Christian-Albrechts University of Kiel, Olshausenstrasse 40, 24098 Kiel, Germany*

Received 18 May 2005; received in revised form 11 September 2006; accepted 23 September 2006
Available online 17 November 2006

Abstract

Zero-valent iron (ZVI) permeable reactive barriers (PRBs) have become popular for the degradation of chlorinated ethenes (CEs) in groundwater. However, a knowledge gap exists pertaining to the longevity of ZVI. The present investigation addresses this situation by suggesting a numerical simulation model that is intended to be used in conjunction with field or column tests in order to describe long-term ZVI performance at individual sites. As ZVI aging processes are not yet completely understood and are still subject to research, we propose a phenomenological modelling technique instead of a common process-based approach. We describe ZVI aging by parameters that characterise the extent and rate of ZVI reactivity change depending on the propagation of the precipitation front through ZVI. We approximate degradation of CEs by pseudo-first order kinetics accounting for the formation of partially dechlorinated products, and describe ZVI reactivity change by scaling the degradation rate constants. Three independent modelling studies were carried out to test the suitability of the conceptual and numerical model to describe the observations of accelerated column tests. All three tests indicated that ZVI reactivity declined with an increasing number of exchanged pore volumes. Measured and modelled concentrations showed good agreement, thereby proving that resolving spatial as well as temporal changes in ZVI reactivity is reasonable.

Keywords: Permeable reactive barrier; Zero-valent iron; Long-term performance; Degradation; Chlorinated hydrocarbons; Reduction of iron reactivity

* Corresponding author. Tel.: +49 7071 2973177; fax: +49 7071 5059.
E-mail address: michael.finkel@uni-tuebingen.de (M. Finkel).

0169-7722/$ - see front matter © 2006 Elsevier B.V. All rights reserved.
doi:10.1016/j.jconhyd.2006.09.014

1. Introduction

To date, zero-valent iron (ZVI) is the material most often proposed and used for the *in-situ* treatment of chlorinated ethenes (CEs) in groundwater (Wilkin et al., 2002). Numerous researchers have reported on the mechanism and kinetics of contaminant degradation by ZVI (e.g., Matheson and Tratnyek, 1994; Bonin et al., 1998; Wüst et al., 1999; Arnold and Roberts, 2000). Recently, researchers have focused on changes in iron reactivity over time and with exposure to groundwater, with variability in such factors as flow rate, influent CE concentrations, inorganic and microbial compositions (Gu et al., 1999; Farrell et al., 2000; Scherer et al., 2000; Köber, 2001; Gavaskar et al., 2002; Agrawal et al., 2002; Klausen et al., 2003; Wilkin and Puls, 2003).

The long-term reactivity of ZVI in remedial systems depends on the continued effectiveness of ZVI to serve as an electron donor (Farrell et al., 2000). Field data from ZVI PRBs indicate that reactive performance of ZVI has not generally been problematic, that is, it has not shown severe deterioration (Reynolds, 2002; Gavaskar et al., 2002; O'Hannesin, 2004). However, even the earliest PRBs have been in service for less than a decade. Consequently, the long-term (decades) reactive performance of ZVI remains unclear.

Laboratory studies provide an important glimpse into the effects of individual groundwater constituents on the iron and indicate the inhibition or acceleration of CEs' degradation related to water chemistry. However, most of the laboratory studies have investigated the effect of a single constituent using artificial solutions (i.e., carbonate species — Agrawal et al., 2002; Klausen et al., 2003; chromate — Schlicker et al., 2000; nitrate — Schlicker et al., 2000; Farrell et al., 2000; Ritter et al., 2003; permanganate — Okwi et al., 2005; silicate — Klausen et al., 2003; Kohn et al., 2005; natural organic matter — Tratnyek et al., 2001; Klausen et al., 2003). Ebert et al. (2006) demonstrated that complex interactions take place in systems using groundwater of more or less complex composition, and cumulative or antagonistic effects on CEs' degradation are not derivable from the plain combination of effects observed in more simple (e.g., single-constituent) experiments.

For a better estimation of the ZVI longevity, some of the experimental studies were supported by modelling (e.g., Hatfield et al., 1996; Liang et al., 1997b; Mayer et al., 2001; Yabusaki et al., 2001; Agrawal et al., 2002; Morrison, 2003). Most of the models presented thus far are process-oriented. They facilitate gaining insight into the processes that are involved in the treatment of contaminants by ZVI, namely: degradation, reduction of other electron acceptors present in the ambient groundwater (Mayer et al., 2001), precipitation of secondary minerals (Mayer et al., 2001; Yabusaki et al., 2001; Gavaskar et al., 2002), parallel iron dissolution reactions and complexation reactions (Yabusaki et al., 2001), microbially mediated sulfate reduction and degassing of hydrogen gas (Mayer et al., 2001). Recent reaction and transport models are capable of simulating decreasing reactivity and permeability, both related to iron consumption and mineral precipitation (Agrawal et al., 2002; Morrison, 2003; Li et al., 2004). However, there are only a few models that are applied to real sites (e.g., Mayer et al., 2001; Yabusaki et al., 2001; Morrison, 2003), and terms describing potential acceleration of degradation velocity are not considered. A precise long-term assessment of ZVI performance has not been possible to date. The chemical reactions occurring at mineral surfaces leading to change of reactivity are poorly understood, as is the effect of mineral precipitation on porosity and permeability. Therefore, a better understanding of these processes is needed to have confidence in ZVI longevity estimations made with the process-oriented models.

In this paper, we propose a modelling approach that attempts to describe and quantify observed phenomena of spatial and temporal changes in ZVI reactivity, rather than specific processes. This

means that the effects of mineral precipitation (mediated by biogeochemical reactions) on the reductive degradation of CEs are described in a lumped way. In doing so, we accept being unable to identify individual processes and influencing factors which alter the ZVI performance at any particular site over time. Subsequently, the setup of such a spatio-temporal simulation model (STS model) is presented. Note that the impact of mineral precipitation on the ZVI performance with respect to porosity reduction is not assessed, as it is typically of minor importance compared to the impact with respect to ZVI reactivity (Gavaskar et al., 2002; Morrison, 2003; Vikesland et al., 2003). As a premise to calibrate the model, it is assumed that meaningful performance data exhibiting ZVI reactivity change are available. In this study, the model is applied to the data of three accelerated column tests, which were conducted with actual groundwater from the sites at the former NAS Moffett Field, USA (Gavaskar et al., 2002), Rheine, Germany (Möller, 1998; Ebert et al., 1999, 2003; see also http://www.rubin-online.de and http://www.rtdf.org for more information on PRB) and Stuttgart, Germany (Ebert et al., 2002). While the focus in the Moffett Field column experiment was on the degradation of trichoroethene (TCE), the Rheine column experiment focused on tetrachloroethene (PCE), TCE and *cis*-1,2-dichloroethene (*cis*-DCE) and the Stuttgart column experiment on PCE, TCE, *trans*-1,2-dichloroethene (*trans*-DCE), *cis*-DCE and vinyl chloride (VC).

2. Method

2.1. Conceptual model

The reductive dechlorination of chlorinated compounds by ZVI is a surface-mediated reaction, commonly described by first-order kinetics with respect to contaminant concentrations (Gillham and O'Hannesin, 1994; Johnson et al., 1996; O'Hannesin and Gillham, 1998). Wüst et al. (1999) observed a zero-order degradation law for high concentrations (>200 μM) of TCE and *cis*-DCE, indicative of surface reaction limitation (Schäfer et al., 2003), that is, limitation in reactive sites and possible hindering of further adsorption and degradation of contaminants. In our numerical investigation, for all column tests, the first-order expression was adopted. For the Moffett Field simulations, Kouznetsova (2006) tested the accuracy of approximating TCE degradation with the first-order expression through comparison with alternatives, such as N-order ($0<N<1$, $N>1$; Liedl et al., 1999) and combined zero-and first-order (Wüst et al., 1999) expressions. Numerical examples demonstrated that, despite the high influent TCE concentration (~668 μM), TCE degradation can be efficiently and accurately simulated by the first-order. For the Rheine and Stuttgart simulations, the first-order expression is adequate, as indicated by the moderate influent contaminant concentrations (Rheine: ~68 μM of PCE, ~2.15 μM of TCE and ~0.70 μM of *cis*-DCE; Stuttgart: ~0.13 μM of PCE, ~21.84 μM of TCE, ~1.15 μM of *trans*-DCE, ~156.8 μM of *cis*-DCE and ~0.14 μM of VC).

Degradation of CEs and other intermediates during reaction on ZVI occurs via three processes, referred to as reductive β-elimination, hydrogenolysis and hydrogenation (Arnold and Roberts, 2000). Most studies have focused on β-elimination, as it is considered to be the dominant process: CEs are degraded to ethane, ethene and acetylene as the primary end products. Only a few studies report partially dechlorinated reaction products (e.g., TCE, *cis*-DCE and VC) that may be formed by more than one route (Orth and Gillham, 1996; Liang et al., 1997a; O'Hannesin and Gillham, 1998; Su and Puls, 1999; Arnold and Roberts, 2000; Farrell et al., 2000). Even though partially dechlorinated species are minor products, they are regarded as contaminants in drinking water and their presence may dictate the overall design of the PRBs (Vogan et al., 1995; Yamane et al., 1995;

Tratnyek et al., 1997; Schäfer et al., 2003). In this study we account for the formation of partially dechlorinated products; however, we do not distinguish the mechanisms or degradation pathways through which they are generated. Therefore, the STS model is a simplified representation of the reaction scheme from Arnold and Roberts (2000), which comprises a unidirectional network of CE degradation reactions on ZVI. Fig. 1 illustrates the reaction scheme for an exemplary system containing four toxic CEs (PCE, TCE, *cis*-DCE and VC). Meta-stable intermediates, such as acetylene and further DCE isomers, typically produced at low amounts, are neglected. According to the scheme, the degradation rate of each chlorinated ethene can be expressed as

$$\frac{dC_j}{dt} = -k_j C_j + \sum_{i}^{p} \kappa_{ij} k_i C_i, \tag{1}$$

where C_i is the aqueous concentration of compound i that degrades to compound j [M L^{-3}], C_j is the aqueous concentration of compound j [M L^{-3}], p is the number of compounds [−] that can degrade to compound j, t is time [T], k_i and k_j are the first-order degradation rate constants (corresponding to reductive elimination plus hydrogenolysis) of compounds i and j [T^{-1}], respectively, and κ_{ij} is the mole percent conversion of compound i to compound j (i.e., branching ratio). The differential equation system is approximated numerically by the finite difference technique (Bayer, 2004; Bayer and Finkel, 2005).

As mentioned above, the dechlorination process may be adversely affected by mineral coatings on ZVI surfaces, due to an inhibition of the electron transfer between ZVI and contaminant species. Long-term column experiments and field observations by different investigators evinced the existence of precipitation accumulation fronts (Farrell et al., 2000; Schlicker et al., 2000; Klausen et al., 2003; Vikesland et al., 2003; Wilkin et al., 2003; Zhang and Gillham, 2005). For instance, Klausen et al. (2003) observed a change in colour (indicative of precipitation) in ZVI columns from an initial dark grey/black to a lighter grey that progressed slowly from the column inlet toward the distal end. Furthermore, Klausen et al. (2003) stated that "at the proximal ends of the columns, apparently unreactive zones grew over time". To simulate a spatial deactivation trend, we assume that a precipitation front moves through ZVI in the flow direction. Ahead of the front, ZVI has its original reactivity; behind the front, in the zone of precipitate accumulation, the reactivity of ZVI is lowered.

The length of the transition zone (*TZ*) between the regions of full and minimum reactivity of ZVI (i.e., the remaining reactivity, RR_j) represents the shape of the precipitation front (Fig. 2), which is expected to be dependent on inorganic water chemistry, reaction kinetics, and flow velocity. For instance, the abiotic reduction of nitrate occurs comparatively fast on ZVI and results in a strong inhibition of CE degradation (Sinatar et al., 1995; Cheng et al., 1997; Rahman and

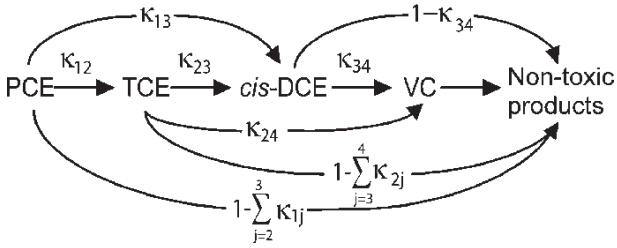

Fig. 1. Sequential degradation of PCE, TCE, *cis*-DCE, and VC.

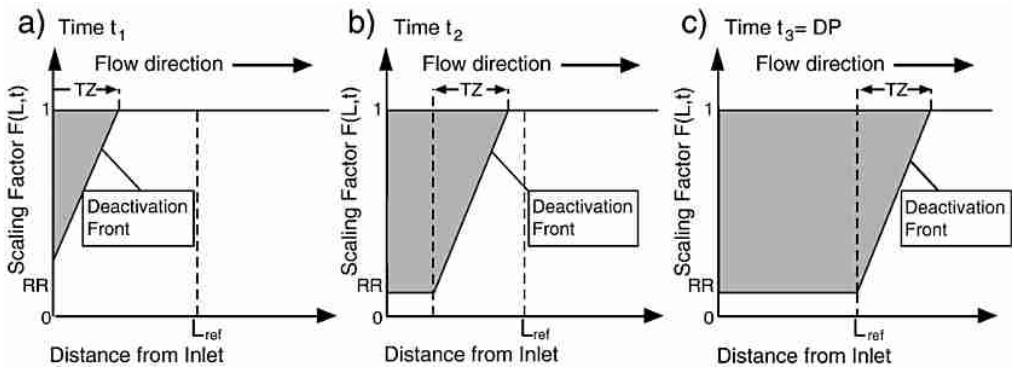

Fig. 2. Conceptual model of ZVI deterioration: propagation of passivation front.

Agrawal, 1997; Farrell et al., 2000; Ritter et al., 2003). Schlicker et al. (2000) observed passivation/precipitation fronts with narrow transition zones moving throughout the columns in experiments with high nitrate or chromate backgrounds. In contrast, carbonate precipitation is often spread over broad distances. Thus, a more even decrease in reactivity could be observed (Klausen et al., 2003; Ebert, 2004), suggesting that a broader transition zone develops in this case.

To simulate a spatial (i.e., along the flow direction) and temporal variability of ZVI reactivity, degradation rate constants of the contaminants, j, are scaled by space-and time-dependent, dimensionless factors, F_j [−], that range from 0 to 1. Recall that our model does not particularly investigate the chemical changes that occur due to iron aging in different geochemical systems. Therefore, the scaling factors are conditioned by such model parameters as: (i) the deactivation period, DP [T], (ii) the remaining reactivity of ZVI, RR_j [−] or [%], and (iii) the length of the transition zone between the regions of full and minimum reactivity, TZ [L]. The change from full to minimum reactivity within the transition zone is assumed to be linear. Since the ZVI aging may have a different effect on the degradation of particular contaminants (Wang and Farrell, 2003), parameter RR_j is expressed compound-specifically. The value of DP serves as a proxy for the propagation velocity of the precipitation front, as DP is the time after which deactivation to RR_j has completely evolved through a reference ZVI flowthrough thickness, L_{ref} [L] (e.g., the column length in the lab studies).

The scaling factors for degradation rate constants $F_j(L,t)$ may be determined as a function of time t [T] and distance L [L] from the ZVI reactor inlet by examining the propagation of the precipitation front. Assigning n as the superscript identifying normalisation to the ZVI cross-sectional area, the following expressions can be formulated:

$$V^n_{\mathrm{ref},j} = L_{\mathrm{ref}} \cdot (1-\mathrm{RR}_j), \tag{2}$$

$$V^n_{\mathrm{TZ},j} = \frac{\mathrm{TZ} \cdot (1-\mathrm{RR}_j)}{2}\ , \text{and} \tag{3}$$

$$V^n_j(t) = \frac{t \cdot (V^n_{\mathrm{ref},j} + V^n_{\mathrm{TZ},j})}{\mathrm{DP}} \tag{4}$$

where $V^n_{\mathrm{ref},j}$ is the *(normalised)* reference ZVI volume [L] deactivated to the minimum level of reactivity RR_j, $V^n_{\mathrm{TZ},j}$ is the *(normalised)* deactivated volume [L] within the transition zone between

regions of full and minimum reactivity RR_j, and $V_j^n(t)$ is the total deactivated *(normalised)* ZVI volume [L] at time t [T].

For early times, that is, when the transition zone has not yet completely evolved in the column ($V_j^n(t) \le V_{TZ,j}^n$, see Fig. 2a), the ZVI flowthrough thickness $L_{max,j}$ [L], up to which the precipitation front has propagated after time t [T], is expressed as:

$$L_{max,j}(t) = \sqrt{\frac{2 \cdot V_j^n(t)}{\theta_j}} \tag{5}$$

where θ_j is the slope [L^{-1}] that characterises F_j within the transition zone and

$$\theta_j = \frac{1-RR_j}{TZ}. \tag{6}$$

$L_{max,j}$ [L] equals TZ [L] when the transition zone has completely propagated into the column. This occurs at time

$$t^* = \frac{TZ}{2L_{ref} + TZ} DP. \tag{7}$$

For later times ($t > t^*$), when $V_j^n(t) > V_{TZ,j}^n$ (see Fig. 2b and c), the relevant expression is

$$L_{max,j}(t) = TZ + \frac{(V_j^n(t) - V_{TZ,j}^n)}{(1-RR_j)}. \tag{8}$$

Finally, the compound-specific scaling factor $F_j(L,t) \in \lfloor RR_j, 1 \rfloor$ is expressed as follows:

$$F_j(L,t) = 1 - \theta_j \cdot (L_{max,j}(t) - L) \text{ for } L \in \left[0, L_{max,j}(t)\right], \tag{9a}$$

$$F_j(L,t) = 1 \text{ for } L > L_{max,j}(t). \tag{9b}$$

Note that, according to the STS model, having TZ greater than ZVI flowthrough thickness of the whole reactor is also possible. This case is a more general interpretation of reactivity transition: minimal and/or maximal reactivity in the model exists as extrapolated references (Fig. 3). As can

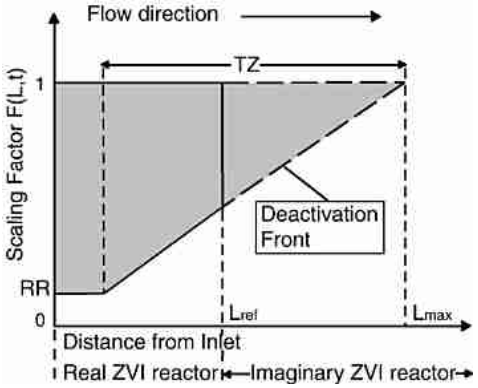

Fig. 3. Extrapolation of maximum reactivity in STS model.

be expected for high groundwater flow velocities or thin walls, reactivity then changes over the entire flowthrough thickness.

It should be mentioned that, according to Zhang and Gillham (2005), precipitate formation appears to be a self-regulating process, with the precipitates causing reduced reactivity, which in turn reduces the rate of precipitate formation (respectively, rate of ZVI deactivation, dV_j^n/dt). In laboratory experiments, Okwi et al. (2005) observed a rapid loss of reactivity that progressed through a column as a moving front, followed by a much slower but progressive loss of reactivity across the entire column. It appears that the phenomenon of changing rate of ZVI deactivation should be incorporated in the models simulating ZVI long-term performance, but knowledge about this phenomenon is not yet sufficient to do so. Therefore, in the STS model we assume that deactivation parameters (RR_j, DP, TZ) and the rate of ZVI deactivation (dV_j^n/dt) are constant over time. Another assumption that we introduce due to the knowledge deficit is that branching ratios are not affected by iron aging. The speculations of other researchers about this issue are presented subsequently in the results and discussion section.

2.2. Model calibration

Compared to other modelling studies (Farrell et al., 2000; Gavaskar et al., 2002; Klausen et al., 2003), an essentially different way of model parameter estimation (i.e., fitting to experimental data) is suggested here. While other investigators calibrated the model parameters against concentration profiles over column distance independently for different exposure times (local time fitting), we perform simultaneous fitting of these data (global fitting). Using all concentration data at once is shown to be a more robust approach which is less susceptible to outliers (see section *NAS Moffett Field column simulations*). The model parameters to be calibrated are initial degradation rate constants (k_j), branching ratios (κ_{ij}), as well as deactivation period (DP), length of transition zone (TZ) and remaining reactivity (RR_j). We solved the calibration by using a heuristic optimisation technique, the derandomised evolution strategy (CMA-ES; Hansen et al., 2003), which is especially useful for nonlinear problems and does not require closed form objective functions. The algorithm is implemented as an external solver that repeatedly calls the STS model. Each model call provides an indication of the ability of the model to reproduce concentration data accurately. Kouznetsova (2006) examined two quantitative measures for the STS model calibration: the absolute logarithmic error, absL and the relative residual mean square error, rRMS. The minimization of the errors was achieved after several hundreds model calls, the input parameters of which were specified iteratively by the heuristic solver. In curve fitting with the rRMS, higher concentrations (at the proximal end of the column) were simulated more accurately than smaller concentrations (at the distal end of the column). It was concluded that absL offers slight advantages compared to rRMS, as it yields a better fit at the distal end of the column, being less biased in favour of fitting higher concentrations. Therefore, in this study the optimal parameter fit for a specific compound is defined as the one producing the minimum $absL_j$ [log(M L^{-3}]:

$$\mathrm{absL}_j = \frac{\sum |\log(C_{j,\mathrm{meas}}) - \log(C_{j,\mathrm{mod}})|}{m} \tag{10}$$

where $C_{j,\mathrm{meas}}$ is the measured and $C_{j,\mathrm{mod}}$ is the modelled concentrations [M L^{-3}] of compound j, and m is the total number of observations [−]. In Eq. (10), it is understood that the summation is carried out with respect to all sampling ports at all sampling times. Fig. 4 summarises the elementary steps of the calibration procedure.

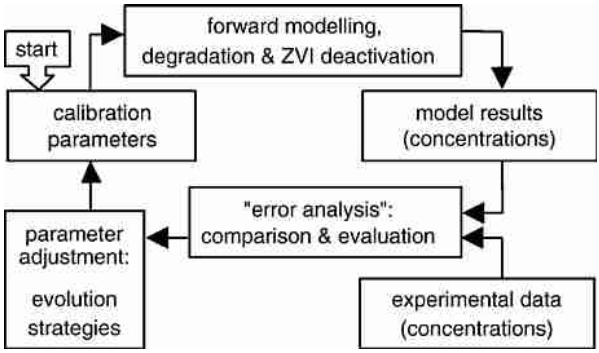

Fig. 4. Flowchart of the calibration procedure.

If there is only one compound of interest (e.g., in the Moffett Field column test), the above-mentioned calibration parameters are adjusted simultaneously, except for branching ratios, which are not relevant in this case. If there is more than one compound (e.g., the Rheine and Stuttgart column tests), simultaneous adjustment of parameters may result in non-uniqueness of the parameter values due to interdependence of degradation rate constants of parent and daughter compounds and branching ratios. Hence, in these cases we chose to derive the parameter values in a stepwise fashion, starting with degradation data for the highest chlorinated ethene and proceeding to the lesser chlorinated ethenes. For instance, if the examined contaminant mixture contains PCE, TCE and *cis*-DCE, then calibration will start with data for PCE degradation and proceed via TCE to *cis*-DCE. After DP, TZ (both independent of CE type) and parameters for the highest chlorinated ethene are calculated; they are retained for use in the calibration process for the next, lesser chlorinated ethene. An assumption embedded in this sequential parameter adjustment is that the degradation rate of a parent compound is not dependent on the number and concentrations of daughter products (i.e., interspecies competition is not considered). The fractions accounting for the degradation of a highly chlorinated ethene to partially dechlorinated byproducts (κ_{ij}) are estimated while adjusting the parameter values of the target ethenes, that is, potential daughter products. Table 1 shows the sequence in which model parameters are derived for the exemplary mixture containing PCE, TCE and *cis*-DCE.

2.3. Model input and model configuration

The values of all model input parameters that were not subject to calibration are specified in accordance to the Moffett Field, Rheine and Stuttgart column tests. Column packing materials and properties, as well as column setup and operating conditions, are listed in Table 2. For further details the reader should refer to Gavaskar et al. (2002), Parbs et al. (2003), Ebert (2004), Ebert et al. (2002).

Table 1
Stepwise calibration for a mixture containing PCE, TCE and *cis*-DCE

Steps	Calibrated parameters
1	k_{PCE}, RR_{PCE}, DP, TZ
2	k_{TCE}, $\kappa_{PCE\text{-}to\text{-}TCE}$, RR_{TCE}
3	$k_{cis\text{-}DCE}$, $\kappa_{PCE\text{-}to\text{-}cis\text{-}DCE}$, $\kappa_{TCE\text{-}to\text{-}cis\text{-}DCE}$, $RR_{cis\text{-}DCE}$

Table 2
Summary of the NAS Moffett Field, Rheine and Stuttgart column tests

	NAS Moffett Field column	Rheine column			Stuttgart Column				
Packing material	Iron (peerless metal powders and abrasives; Detroit, Michigan)	Grey cast iron (Gotthart Mayer, AG) (33 vol.%) and gravel			Grey Cast Iron (Gotthart Mayer, AG)				
Porosity*	0.64	0.37			0.40				
Operation time*	274 days/1300 PV	420 days/242 PV			205 days/49 PV				
Column dimensions*	91.4 cm × 3.8 cm I.D	97 cm × 10 cm I.D.			101.5 cm × 10 cm I.D.				
Locations of sampling ports	Distance from inlet (cm)*								
	0; 15.2; 30.5; 45.7; 61.0; 91.4	0; 3; 8; 13; 22; 32; 47; 62; 77; 92; 97			0; 1.5; 6.5; 11.5; 21.5; 31.5; 46.5; 61.7; 76.6; 91.5				
Sampling events	Days from the start of the test* (pore volumes)								
	5(42); 10(84); 17(140); 22(187); 27(223); 31(257); 38(317); 76(475); 205(1012); 213(1047); 273(1295)	4(2); 27(16); 46(27); 67(39); 96(55); 111(64); 145(84); 166(96); 220(127); 293(169); 312(180); 361(208); 420(242)			16(4); 35(8); 57(14); 78(19); 99(24); 125(30); 154(37); 181(44); 205(49)				
Operating conditions									
Concentrations*	TCE ($mg\ L^{-1}$)	PCE ($\mu g\ L^{-1}$)	TCE ($\mu g\ L^{-1}$)	*cis*-DCE ($\mu g\ L^{-1}$)	PCE ($\mu g\ L^{-1}$)	TCE ($\mu g\ L^{-1}$)	*trans*-DCE ($\mu g\ L^{-1}$)	cis-DCE ($\mu g\ L^{-1}$)	VC ($\mu g\ L^{-1}$)
Influent	69.4–1260	7795–13,324	44–803	49–102	5.4–59.3	993–5440	33.1–157	6525–20,635	0–38.3
Effluent	19.7–79.6	1–7519	1–317	1.4–205	<1	<1	<1	60–4298	7–186
Flow rate*	3.8 mL min^{-1} until 317 PV, 1.9 mL min^{-1} until 1300 PV	1.02 – 1.29 mL min^{-1}			0.63 – 1.10 mL min^{-1}				

* Input parameters used in the STS Model.

Each column experiment was simulated using a one-dimensional transient flow and transport model. The measured values of the volumetric flow rate and CE inflow concentrations were used to describe the boundary conditions. Contaminant transport was assumed to be purely advective (plug flow). A finite difference grid spacing of $\Delta x = 1$ cm was used to discretise the column length. The time step length Δt [T] was adjusted automatically according to $\Delta t = \Delta x / v$, with v [L/T] being the flow velocity. (Courant criterion for the model equals 1). Changing operation conditions were resolved by time intervals of 4 to 7 days depending on the duration of the particular experiment. The chosen discretisation was proven to be appropriate, as preliminary calculations with finer discretisations (e.g., $\Delta x = 1$ mm and time interval of 1 day) showed the same results. That is, the values of the fitted parameters and absL were the same. According to the ZVI flowthrough thickness in the columns, the reference thickness for the evaluations of ZVI aging was set to $L_{ref,Moffett} = 92$ cm, $L_{ref,Rheine} = 97$ cm and $L_{ref,Stutt} = 101.5$ cm.

Please note that, following the recommendation of Gavaskar et al. (2002), in the NAS Moffett Field column we excluded from calibration the data collected at 42 and 317 pore volumes. For the former case, early concentration data was shown to be biased by sorption to non-reactive sites. Since this is not accounted for in the STS model, it would have resulted in an overestimation of the fitted rate constants had the data been included. In the latter case, concentration data were taken shortly after the flow rate had been abruptly adjusted from 3.8 mL min^{-1} to 1.9 mL min^{-1} thus reflecting exceptional non-equilibrium conditions which render the data unsuitable for calibration. Following the recommendation of Gavaskar et al. (2002) further, we did not consider measured influent and effluent concentrations in the calibration, thereby avoiding column end effects that bias the calculations of the degradation rate constants (i.e., abrupt change in diameter between the tubing and the column; accumulation of the gas bubbles in the effluent end of the column). For the Rheine and Stuttgart column simulations, the model parameters were fitted excluding the influent measured concentrations from calibration. Concentrations measured at 2 and 16 pore volumes for the Rheine column and at 4 pore volumes for the Stuttgart column were also excluded, because the concentration profiles indicated that sorption sites were not sufficiently saturated and there were strong non-equilibrium conditions in the columns. Furthermore, the apparent outliers in measured concentrations were excluded. The outliers were determined on the basis of standard deviations, σ, calculated using three parallel samples that were taken at each sampling port (if σ is greater than 10%, the concentration measurement is not considered). In the Rheine column, the outliers comprise 11.8% of the evaluated data and in the Stuttgart column −6.7%.

3. Results and discussion

3.1. NAS Moffett Field column simulations

The breakthrough curves of modelled effluent TCE concentrations compared to column influent and effluent TCE concentrations are shown in Fig. 5 (here “effluent” is understood as the concentration at the last port, as it is more meaningful than the concentration at the column end (according to Gavaskar et al., 2002)). Effluent TCE concentration showed a decrease over influent concentration, as was expected due to TCE degradation by ZVI. Fig. 5 exemplifies the best-fit profile for TCE effluent, illustrating that both the measured and the modelled effluent TCE concentrations are in good agreement throughout the exchange of 1300 pore volumes. Additional plots of concentration profiles for different times are presented in Fig. 6. The corresponding best-fit model parameters are listed in Table 3. To give an estimate of the uncertainty in the fitted

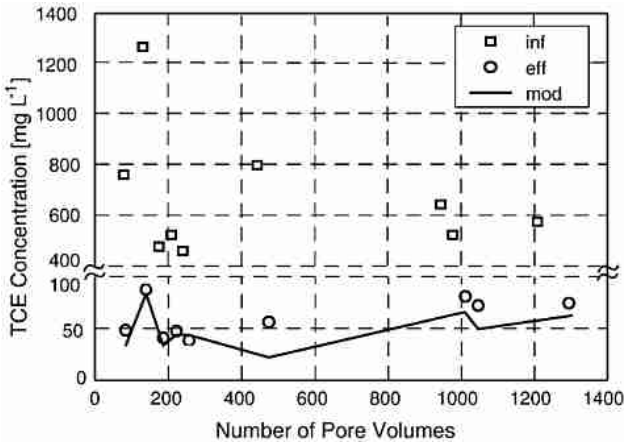

Fig. 5. Breakthrough curves of modelled (mod) effluent TCE concentration compared to observed influent (inf) and effluent (eff) concentrations for the NAS Moffett Field column. Column data from Gavaskar et al. (2002).

parameters, Monte-Carlo simulations were performed (i.e., parameters were varied randomly and simultaneously within a 25% range of each best-fit parameter value). This way, 10000 alternative parameter settings were evaluated. All settings that yield an absL error not higher than 2% above the absL error of the best-fit setting were counted as 'acceptable' and were further analysed with respect to the parameter ranges. The bounds of these ranges (min and max) are also listed in Table 3. The ranges of the individual parameters normalised to the corresponding best-fit value indicate that the accuracy of the model fit is particularly sensitive for k_{TCE} and RR_{TCE}, whereas the impacts of DP and TZ are moderate and low, respectively. Please note that the size of the parameter ranges is governed by the error tolerance used. This issue will be highlighted further below in the example of the Rheine column simulations.

It should be mentioned that, according to Gavaskar et al. (2002), it is possible that in the first part of the Moffett Field column test (until 317 pore volumes) precipitate formation and retention had not reached their maximum in the column. The colloidal precipitate particles were washed out of the column before the reduction of the water flow rate from 3.8 mL min^{-1} to 1.9 mL min^{-1} at 317 pore volumes. However, after the flow rate reduction, all the precipitates generated were retained in the column. Based on the fact that the data fit is good at all times (Fig. 6), we presume that the effects of varying the flow rate do not significantly influence the accuracy of the ZVI longevity estimation (i.e., the calibrated parameters).

It is instructive to compare the TCE degradation parameters calibrated using the STS model with those obtained by means of local fitting of the pseudo-first order model, assuming spatially constant degradation (i.e., rate constants are constant irregardless of position within the column). The results of this comparison are shown in Fig. 7. Spatially constant degradation rate constants k_{SC} are provided for specific times of TCE concentration measurements (see also the best-fit exponential regression line $k_{SC,trend}$). The spatially varying (i.e., profiled), degradation rate of the STS model is described by three values: (i) the minimum value of the rate constant, $k_{STS,min}$ (at the column inlet), (ii) the maximum value, $k_{STS,max}$ (at the column outlet), and (iii) the effective value, $k_{STS,eff}$. The latter is the uniform equivalent of the rate constant profile of the STS model (i.e., the rate constant that gives the same TCE concentration at the column outlet as the one calculated on the basis of the spatially non-uniform rate constant profile). Note that the effective

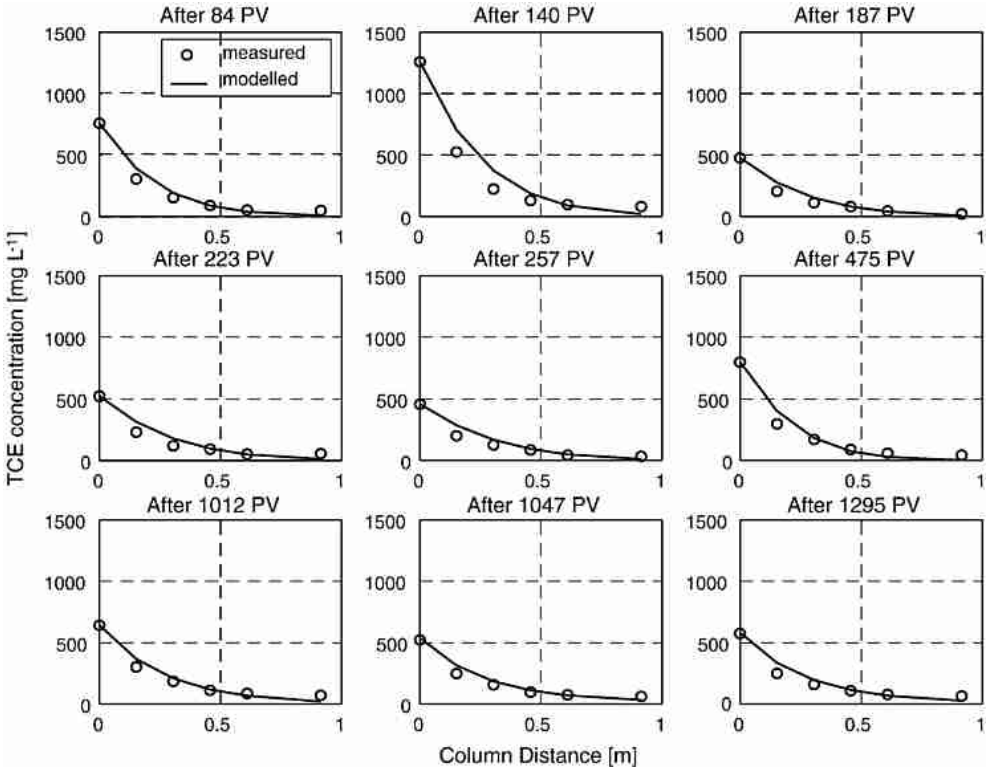

Fig. 6. Modelled (solid lines) and measured (markers) spatial concentration profiles for TCE in the Moffett Field column at different pore volume ages. Note that the plots show influent and effluent concentrations that were not considered in calibration.

rate constant proved to be equivalent to the arithmetic mean of the rate constant profile. The propagation of the passivation front through the column is completely reflected by the development of $k_{STS,min}$ and $k_{STS,max}$ over time. The bend in the $k_{STS,max}$ at 170 pore volumes indicates the point in time when the front (i.e., the transition zone) has reached the column outlet. The time when the transition zone has completely propagated into the column corresponds to the bend in the $k_{STS,min}$ at 533 pore volumes. The reason the transition zone reaches the column outlet prior to its complete propagation into the column is the greater length of the transition zone compared to the column length (comp. Tables 2 and 3). After 1110 pore volumes, $k_{STS,min}$ coincides with $k_{STS,max}$, indicating that the whole column ($L_{ref,Moffett}$) is deactivated to the remaining ZVI reactivity toward TCE, RR_{TCE}. The degradation rate constant of TCE decreases during the course of the experiment from 1.71 h^{-1} to 0.57 h^{-1}, according to the STS. Fig. 7 shows that the margin of the k_{STS} profile encases all locally fitted rate constants except one (at 317 pore volumes). Compared to the scatter of the locally fitted rate constants (k_{SC}), global fitting of the STS model yields a clear and more realistic trend. It is apparent that, especially for a low number of concentration measurements and a broad spread of locally fitted rate constants, an overall trend line can hardly be adapted.

As mentioned above, the STS model determined that after the exchange of 1110 pore volumes (see Fig. 7, or DP in Table 3), the TCE degradation reaches a steady value. The latter could signify

Table 3
Summary of optimised parameters for the Moffett field simulations

Parameters	Symbols	Units	Best-fit	Ranges for other 'acceptable' settings	
				Min	Max
Initial degradation rate constant	k_{TCE}	[h^{-1}]	1.71	1.64	1.90
Remaining reactivity	RR_{TCE}	[%]	33	30.5	35.5
Deactivation period	DP	[days]/[PV]	226/1110	190/949	262/1259
Length of transition zone	TZ	[m]	1.6	1.49	1.66

a quasi steady-state situation, where further accumulation of precipitates does not result in a remarkable decline in surface area concentration of ZVI within the observation period. These observations are consistent with data for TCA reduction reported by Agrawal et al. (2002), in which sustained ZVI reactivity toward TCA was observed after extensive accumulation of $FeCO_3$ on the iron surface. Agrawal et al. (2002) suggested a model assuming that the TCA reduction rate decays exponentially (to a nonzero limit) with C(IV) exposure time. They mentioned reactive Fe^{2+} sites, green rust, pits, pores, and crevices in the precipitate layer as possible explanations for sustained ZVI reactivity. In general, instead of a linear change of the reaction rates, an exponential change could be specified for the STS model. Due to the satisfactory data fit for the Moffett Field column (Figs. 5 and 6), the simpler linear change was preferred.

3.2. Rheine column simulations

Fig. 8 presents graphical results of the stepwise calibration procedure and Table 4 lists the best-fit parameters for the Rheine simulations. The calibration results for the STS model indicate that in this experiment, TCE has the highest initial rate constant ($k_{TCE}=0.228\ h^{-1}$) compared to PCE ($k_{PCE}=0.122\ h^{-1}$) and *cis*-DCE ($k_{cis\text{-}DCE}=0.046\ h^{-1}$), which is typical for the type of iron used

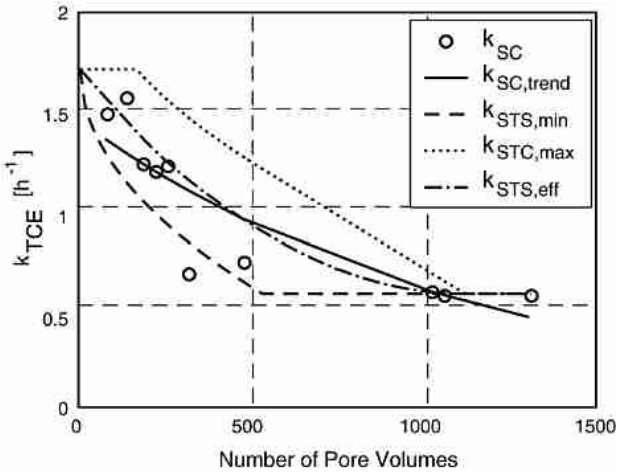

Fig. 7. The pseudo-first order TCE rate constants vs. the number of exchanged pore volumes in the NAS Moffett Field column. Spatially constant TCE rate constants k_{SC} (markers) and the corresponding best-fit exponential trend $k_{SC,trend}$ (solid line) are compared to TCE rate constants determined by the STS model, i.e., minimum $k_{STS,min}$ (dashed line), maximum $k_{STS,max}$ (dotted line) and effective $k_{STS,eff}$ (dashdot line).

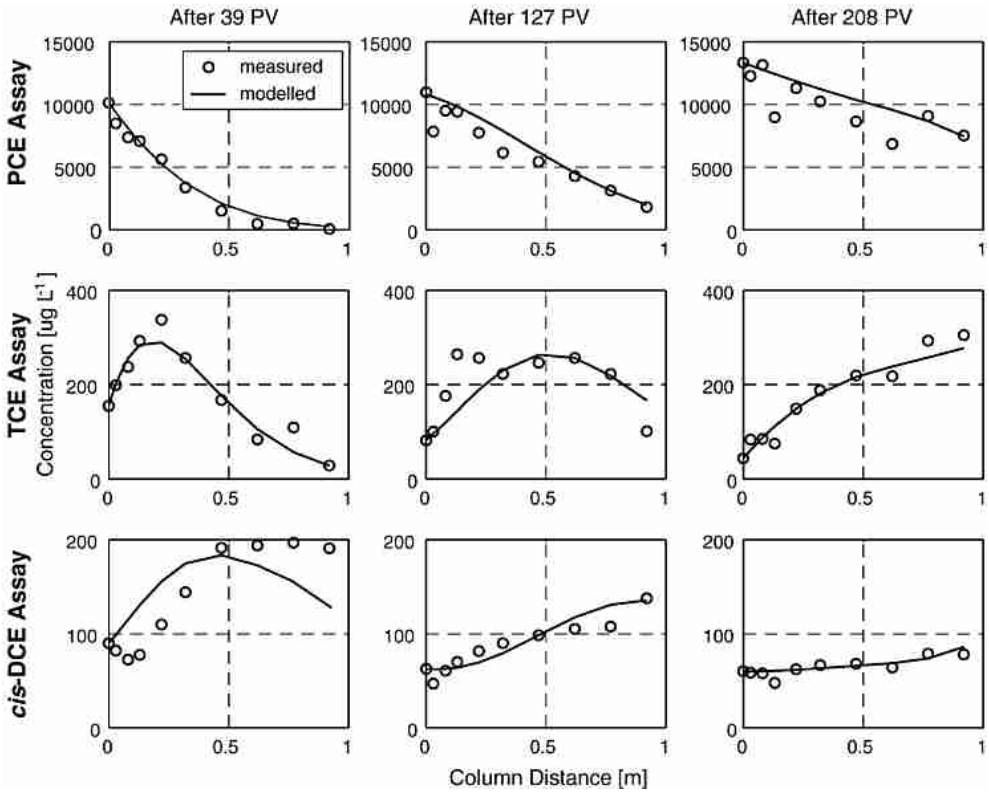

Fig. 8. Modelled (solid lines) and measured (markers) spatial concentration profiles for PCE, TCE and *cis*-DCE in the Rheine column at different pore volume ages.

(Ebert, 2004). It is interesting to make a further comparison with the rate constants reported by other researchers. According to Johnson et al. (1996), by using surface area normalized rate constants (k_{SA}), it is possible to make generalisations about degradation rates by iron metal that apply over a wide range of laboratory conditions. The surface area in the Rheine experiment is 1.21 m^2 mL^{-1}. Compared to k_{SA} presented by Johnson et al. (1996), the average k_{SA} calculated by the STS model are smaller for the degradation of PCE and TCE. Other studies have also shown

Table 4
Summary of optimised parameters for the Rheine simulations

Parameters	Symbols	Units	Compounds		
			PCE	TCE	*cis*-DCE
Initial degradation rate constant	k	[h^{-1}]	0.122	0.228	0.046
Remaining reactivity	RR	[%]	11.5	17.9	95.0
Branching ratio	$\kappa_{PCE\text{-}to\text{-}TCE}$	[%]	11.8		
	$\kappa_{PCE\text{-}to\text{-}cis\text{-}DCE}$	[%]	5.0		
	$\kappa_{TCE\text{-}to\text{-}cis\text{-}DCE}$	[%]	25.5		
Deactivation period	DP	[days]/[PV]	443/255		
Length of transition zone	TZ	[m]	1.7		

more rapid degradation of TCE (Wüst et al., 1999; Su and Puls, 1999; Miehr et al., 2004), while comparable or smaller *cis*-DCE degradation rate constants were determined (Johnson et al., 1996; Wüst et al., 1999). Fig. 9 presents the results of the comparison of surface area normalised first-order rate constants. Additionally, the values of k_{SA} identified by the STS model for the Stuttgart column are shown (the surface area in the Stuttgart experiment is 1.75 m^2 mL^{-1}.). Please note that, due to the mixture of iron and gravel used in the Rheine column, the observed reaction kinetics are slow compared to other experiments using the same granulate iron (Fig. 9 — Stuttgart grey cast iron; Ebert, 2004). However, weighting k_{SA} identified by the STS model with the volume fraction of iron (33%) eliminates the differences (corrected $k_{SA,PCE}=3.07\cdot10^{-4}$ L m^{-2} h^{-1}, $k_{SA,TCE}=5.73\cdot10^{-4}$ L m^{-2} h^{-1}, $k_{SA,cis\text{-}DCE}=1.15\cdot10^{-4}$ L m^{-2} h^{-1}).

The values of RR_j serve as an indicator of the susceptibility of compound-specific iron reactivity to aging. The lower values for PCE ($RR_{PCE}=11.5\%$) and TCE ($RR_{TCE}=17.9\%$) evince a higher reactivity decrease for these contaminants compared to the small decline for *cis*-DCE ($RR_{cis\text{-}DCE}=95.0\%$). We acknowledge, however, that in this specific case the STS model may not provide accurate values for the *cis*-DCE degradation rate constant and the remaining reactivity, $RR_{cis\text{-}DCE}$. Due to the relatively small ZVI flowthrough thickness (97 cm), degradation of *cis*-DCE is obscured by *cis*-DCE production from PCE and TCE. In Fig. 8, a continuous increase of the *cis*-DCE concentrations can be observed with increasing distance from the column inlet, which impedes a distinct interpretation of the data. The PCE and TCE fractions degrading to *cis*-DCE cannot be determined accurately here either, as the net *cis*-DCE production is strongly dependent on the goodness of fit of *cis*-DCE degradation. The Rheine experimental setup (i.e., ZVI flowthrough thickness) was sufficient to describe production of TCE. Although different ZVI types may exhibit completely different reactivities, the fraction of PCE degrading via hydrogenolysis to TCE, reported herein (see Table 4, $\kappa_{PCE\text{-}to\text{-}TCE}=11.8\%$), compares closely to that reported in batch studies by Arnold and Roberts (2000), who concluded that hydrogenolysis accounts for 13% of PCE.

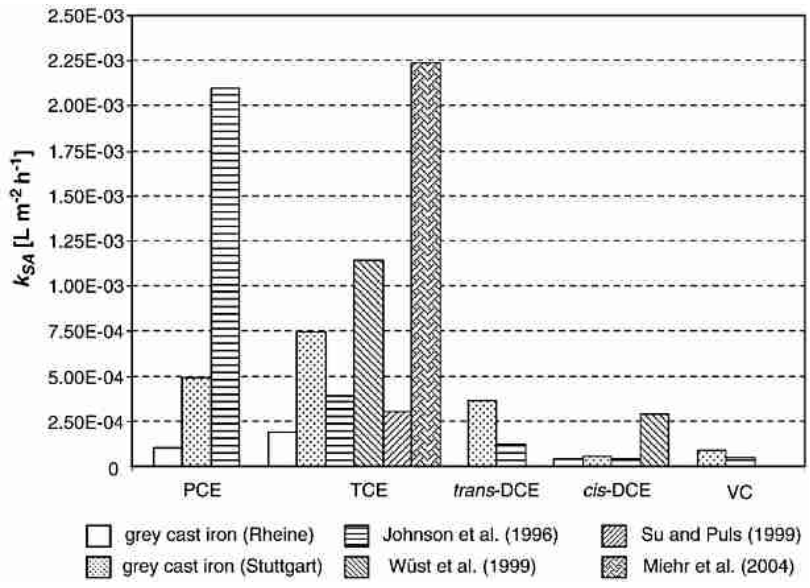

Fig. 9. Comparison of surface area normalised first-order rate constants.

Some researchers have stated that branching ratios might change with ZVI aging (Farrell et al., 2000; Gavaskar et al., 2002). For instance, Gavaskar et al. (2002) supposed that with accumulation of precipitates, the hydrogenolysis pathway replaces β-elimination as the dominant degradation mechanism. One consequence of this replacement is that chlorinated by-products would be produced in greater quantities. On the other hand, Wang and Farrell (2003) noted that cessation of hydrogenolysis may occur if there is competition for hydrogen (i.e., by sulphate reducers). However, for the experimental data analysed here, a simplified approach using constant branching ratios proves to be sufficient, as shown by a good visual fit of modelled and measured concentrations (Fig. 8). Note that constant branching ratios are not an obligatory limitation of the STS model. Transient branching ratios may also be integrated.

The calibrated STS model indicates that the ZVI deactivation does not reach a limit before the end of the experiment on day 420 (242 pore volumes). It is identified by the deactivation period DP that degradation rates are expected to reach steady values after 255 pore volumes (Table 4). Therefore, we can conclude that at the end of the experiment (i) the precipitation front did not propagate through the entire ZVI flowthrough thickness, and (ii) part of the column, namely from the column distance of 88 cm from the inlet up to the column outlet at 97 cm, was within the transition zone.

Using the procedure described above for the Moffett Field column, ranges of model parameters were identified for subsets of parameter settings that meet the given error tolerance of 5%, 2% and 1%. Table 5 provides a summary of the results. It is shown that the size of the subsets considerably decreases for the more stringent error tolerance. And even for the rather loose tolerance of 5%, the range of all parameters is narrowed compared to the original range of variation (50%). The size of the range and its change with decreasing error tolerance gives an indication of the significance of the individual parameters. A comparison of individual parameters' relative ranges (range/best-fit value) reveals that DP and k_{PCE} have the highest impact on the accuracy of the model fit. k_{TCE} and $k_{cis\text{-}DCE}$ have lower impacts compared to k_{PCE}. Similarly, RR_{TCE} and $RR_{cis\text{-}DCE}$ have lower impacts when compared to RR_{PCE}. This is explained by the fact that model parameters for TCE and *cis*-DCE are dependent on the model parameters for PCE, due to the partial dechlorination of PCE to TCE and *cis*-DCE. As mentioned above, *cis*-DCE degradation and production by higher chlorinated ethenes cannot be described accurately due to experimental setup. Therefore, no

Table 5
Summary of the random and simultaneous parameter variation for the Rheine column

	DP [PV]	TZ [m]	RR_{PCE} [%]	k_{PCE} [h^{-1}]	RR_{TCE} [%]	k_{TCE} [h^{-1}]	$\kappa_{PCE\text{-}to\text{-}TCE}$ [%]	$RR_{cis\text{-}DCE}$ [%]	$k_{cis\text{-}DCE}$ [h^{-1}]	$\kappa_{PCE\text{-}to\text{-}cis\text{-}DCE}$ [%]	$\kappa_{TCE\text{-}to\text{-}cis\text{-}DCE}$ [%]
Best-fit (BF)	255	1.7	11.5	0.122	17.9	0.228	11.8	95.0	0.046	5	25.5
Error tolerance: 5% (Number of selected parameter sets: 135 out of 10,000)											
Range Min	205	1.29	8.71	0.104	13.44	0.172	8.90	72.29	0.0346	3.76	19.28
Max	314	1.87	14.37	0.151	22.34	0.278	14.71	99.61	0.0527	5.22	31.69
Range/BF	0.4273	0.3365	0.4922	0.3875	0.4972	0.4649	0.4924	0.2876	0.3935	0.2920	0.4967
Error tolerance: 2% (Number of selected parameter sets: 21 out of 10,000)											
Range Min	212	1.36	9.83	0.116	15.58	0.184	9.39	72.96	0.0347	3.76	19.28
Max	287	1.85	14.27	0.142	22.31	0.254	14.7	99.07	0.0466	4.32	31.57
Range/BF	0.2941	0.2882	0.3861	0.2131	0.3760	0.3070	0.45	0.2748	0.2587	0.1120	0.4820
Error tolerance: 1% (Number of selected parameter sets: 8 out of 10,000)											
Range Min	219	1.37	10.21	0.125	15.91	0.184	9.55	74.59	0.0349	3.77	21.50
Max	265	1.85	14.27	0.142	22.31	0.243	13.42	97.41	0.0418	4.32	29.36
Range/BF	0.1804	0.2824	0.3530	0.1393	0.3575	0.2588	0.3280	0.2402	0.15	0.11	0.3082

reliable conclusions can be made regarding the significance of the uncertainty in the *cis*-DCE model parameters (i.e., $RR_{cis\text{-DCE}}$, $k_{cis\text{-DCE}}$, $\kappa_{PCE\text{-to-}cis\text{-DCE}}$, $\kappa_{TCE\text{-to-}cis\text{-DCE}}$). k_{TCE}, $\kappa_{PCE\text{-to-}TCE}$ and RR_{TCE} (in the order of decreasing significance) have a moderate impact on the ZVI longevity estimation. TZ has the lowest impact.

3.3. Stuttgart column simulations

The set of parameters reflecting the CEs degradation behavior in the Stuttgart column is given in Table 6 (best-fit values as well as the min/max values for an error tolerance of 2%). The graphical results of the parameter optimisation procedure are presented in Fig. 10. With influent PCE concentrations between 5 μg L^{-1} and 60 μg L^{-1} and *trans*-DCE concentrations between 33 μg L^{-1} and 157 μg L^{-1}, degradation of these CEs to under the detection limit could be observed in the first third of the ZVI flowthrough thickness (Fig. 10). TCE also degraded to under the detection limit at approximately the same flow distance, although the influent concentrations of TCE were much higher than those of PCE and *trans*-DCE (i.e., between 1206 μg L^{-1} and 4747 μg L^{-1}). In contrast to PCE, TCE and *trans*-DCE, degradation of *cis*-DCE and VC was observed along the entire ZVI flowthrough thickness. The calibration results for the STS model indicate that in the Stuttgart experiment, similar to the Rheine experiment, TCE has the highest initial degradation rate constant (k_{TCE}=1.3 h^{-1}) and *cis*-DCE the lowest ($k_{cis\text{-DCE}}$=0.09 h^{-1}) compared to the other CEs. At the same time, *cis*-DCE degradation is most affected by ZVI aging ($RR_{cis\text{-DCE}}$=18.5%). ZVI also exhibits a pronounced loss in reactivity towards PCE (RR_{PCE}=20.7%) and medium loss towards TCE (RR_{TCE}=50.7%), *trans*-DCE ($RR_{trans\text{-DCE}}$=61.5%) and VC (RR_{VC}=80%). The impact of ZVI aging on the CEs degradation in the Stuttgart experiment can be demonstrated, for instance, on the VC degradation profiles (Fig. 10). The

Table 6
Summary of optimised parameters for the Stuttgart simulations

Parameters	Units	Symbols	Best-Fit	Ranges for other 'acceptable' settings	
				Min	Max
Initial degradation rate constants	[h^{-1}]	k_{PCE}	0.85	0.69	0.90
		k_{TCE}	1.3	1.13	1.52
		$k_{trans\text{-DCE}}$	0.64	0.59	0.78
		$k_{cis\text{-DCE}}$	0.09	0.07	0.11
		k_{VC}	0.15	0.12	0.18
Remaining reactivities	[%]	RR_{PCE}	20.7	15.9	25.3
		RR_{TCE}	50.7	39.5	63.1
		$RR_{trans\text{-DCE}}$	61.5	55.4	71.5
		$RR_{cis\text{-DCE}}$	18.5	14.5	21.6
		RR_{VC}	80	61.9	94.5
Branching ratios	[%]	$\kappa_{PCE\text{-to-}TCE}$	35.6	27.0	44.2
		$\kappa_{PCE\text{-to-}trans\text{-DCE}}$	1.3	1.1	1.6
		$\kappa_{PCE\text{-to-}cis\text{-DCE}}$	22.1	16.6	27.6
		$\kappa_{TCE\text{-to-}trans\text{-DCE}}$	2.7	2.0	3.1
		$\kappa_{TCE\text{-to-}cis\text{-DCE}}$	1.5	1.2	1.8
		$\kappa_{trans\text{-DCE-to-VC}}$	12.3	9.9	13.8
		$\kappa_{cis\text{-DCE-to-VC}}$	4.7	3.6	5.1
Deactivation period	[days]/[PV]	DP	402/96	382/91	492/117
Length of transition zone	[m]	TZ	0.91	0.80	1.1

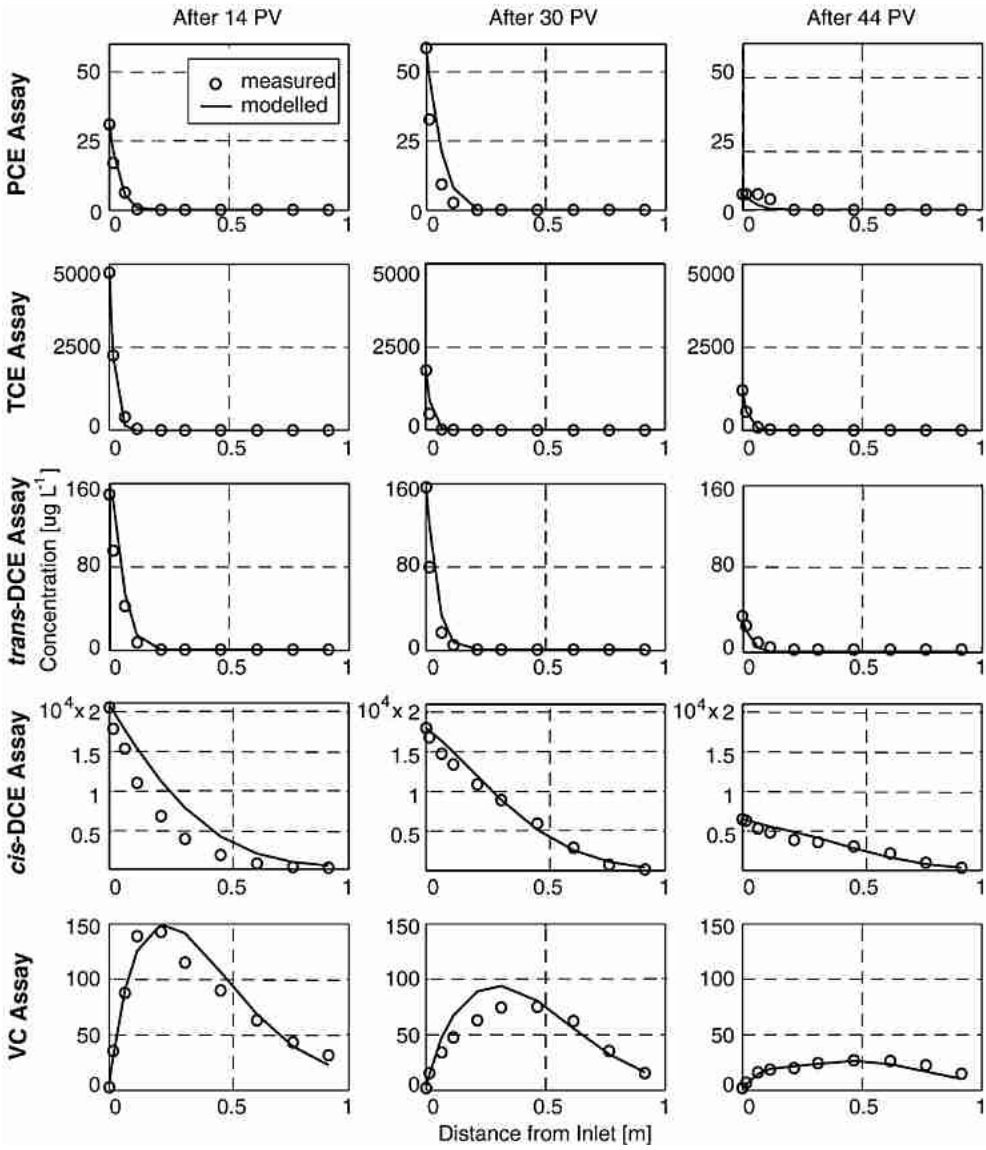

Fig. 10. Modelled (solid lines) and measured (markers) spatial concentration profiles for PCE, TCE, *trans*-DCE, *cis*-DCE and VC in the Stuttgart column at different pore volume ages.

influent VC concentrations were near zero and the effluent concentrations between 15 μg L^{-1} and 31.6 μg L^{-1}. In each VC concentration profile, an increase in the VC concentrations up to a maximum of 143 μg L^{-1} was observed, followed by a decrease. The VC quantities produced by higher chlorinated ethenes became smaller over the duration of the experiment, so that, at the end of the experiment, an increase in VC concentrations by only 27 μg L^{-1} was measured.

The Stuttgart experimental setup (inflow CE concentrations, ZVI flowthrough thickness) differs favourably from the Rheine setup, as the branching ratios can be determined accurately (Table 6). The branching ratio of PCE to TCE and of *trans*-DCE to VC identified by the STS

model are larger than those observed by other investigators (e.g., from Arnold and Roberts (2000), <13% and 1%, respectively). However, the branching ratios of PCE to DCE isomers are comparable to those anticipated by Arnold and Roberts (2000) if branching ratios were to favor hydrogenolysis products to the exclusion of the reductive elimination products (>26%). The branching ratios of TCE and *cis*-DCE to lesser chlorinated ethenes are similar to the branching ratios obtained in column (Orth and Gillham, 1996; O'Hannesin and Gillham, 1998) and batch (Arnold and Roberts, 2000) studies (i.e., 3–6% of the parent compound).

As in the Rheine column simulations, we can conclude, on the basis of the DP value (Table 6), that at the end of the Stuttgart experiment i) the precipitation front did not propagate through the entire ZVI flowthrough thickness, and ii) part of the column, namely from the column distance of 30 cm from the inlet up to the column outlet at 101.5 cm, was within the transition zone. The calibrated STS model indicates that the remaining ZVI reactivity is from 20.7% to 83.5% towards PCE, 50.7% to 89.8% towards TCE, 61.5% to 92.0% towards *trans*-DCE, 18.5% to 83.1% towards *cis*-DCE and 80% to 95.8% towards VC after an exposure to 49 pore volumes. Lower limits of ranges refer to the column inlet and upper limits to the column outlet. The ZVI reactivity decline is expected to reach steady values along the entire ZVI flowthrough thickness after 96 pore volumes.

4. Summary and conclusions

This study focuses on the development of a model for the simulation of the degradation of chlorinated ethenes by ZVI undergoing aging. The main goal is an exact reproduction of contaminant concentration changes in ZVI, as they determine the required ZVI flowthrough thickness for achieving certain remediation targets. The conceptual model proposed here is grounded on the findings of previous studies of the spatial and temporal changes in the contaminant degradation capacity of ZVI when used for groundwater clean-up. Moreover, the model is based on our observations of the movement of zones of maximal, transitional and minimal ZVI reactivity in flow direction through iron columns. The formation of these zones is expected to be due to long-term passivation processes mainly caused by surface precipitation of inorganic constituents, and controlled by iron type and groundwater chemistry. The formulated numerical spatio-temporal simulation (STS) model was calibrated to concentration data from three accelerated column tests (Moffett Field, Rheine and Stuttgart). Taking the entire data set into account during calibration (global fitting), a high level of agreement between calculated and measured concentration profiles of CEs has been achieved for all three cases. Best-fit values of model parameters as well as parameter ranges for alternative parameter settings yielding a given error tolerance were reported. The parameter ranges provide a first estimate of the significance of individual parameters. The narrowness of ranges at stringent error tolerance indicates that the modeling gives reasonably well behaved results. A thorough parameter analysis, however, was beyond the scope of this paper. A comprehensive testing of parameters' sensitivity and uncertainty, including possible interdependencies (e.g., by multivariate statistics, correlation analysis) will follow.

It should be noted that accelerated column tests differ in some respects from flow systems in the field PRBs. For instance, because of the accelerated flow rate in the columns, mineral precipitates are distributed along a longer distance than would normally occur in a field barrier, where sharper deactivation fronts and longer deactivation periods could be expected. In our study, despite possible limitations in transferring the ZVI aging in the columns to the ZVI aging in the field PRB, accelerated column tests were considered to be the best way of obtaining a direct

determination of any future change in iron reactivity. The model has been found to reliably describe conditions observed in the laboratory experiments. However, limited field data exist to confirm that the model can simulate long-term field conditions. Accordingly, additional research and monitoring are necessary to check if the performance anticipated from this study can be transferred to the field.

List of symbols and abbreviations

AFB	Air Force Base
CEs	chlorinated ethenes
DCE	dichloroethene (*trans*-, *cis*-)
PCE	tetrachloroethene
PRBs	permeable reactive barriers
PV	pore volumes
STS	spatio-temporal simulation
TCA	1,1,1-trichloroethane
TCE	trichloroethene
VC	vinyl chloride
ZVI	zero-valent iron
$absL_j$	absolute logarithmic error [$\log(M\ L^{-3})$]
C_i	aqueous concentration of compound i that degrades to compound j [$M\ L^{-3}$]
C_j	aqueous concentration of compound j [$M\ L^{-3}$]
$C_{j,meas}$	measured concentration of compound j [$M\ L^{-3}$]
$C_{j,mod}$	modelled concentration of compound j [$M\ L^{-3}$]
DP	deactivation period [T]
F_j, $F_j(L,t)$	compound-specific scaling factor for degradation rate constant [−]
k_i, k_j	first-order degradation rate constant [T^{-1}]
k_{SA}	surface area normalised rate constant [$L^2\ T^{-1}$]
k_{SC}	spatially constant degradation rate constant [T^{-1}]
$k_{SC,trend}$	spatially constant degradation rate constant calculated by exponential regression [T^{-1}]
$k_{STS,min}$	minimum degradation rate constant (at the column inlet) calculated by the STS model [T^{-1}]
$k_{STS,max}$	maximum degradation rate constant (at the column outlet) calculated by the STS model [T^{-1}]
$k_{STS,eff}$	effective degradation rate constant calculated by the STS model [T^{-1}]
$L_{max,j}$	ZVI flowthrough thickness up to which the precipitation front has propagated [L]
L_{ref}	reference ZVI flowthrough thickness [L]
m	number of measurements [−]
n	superscript identifying normalisation to the ZVI cross-sectional area [−]
N	reaction order [−]
p	number of compounds that can degrade to compound j [−]
RR_j	remaining reactivity of ZVI [−] or [%]
rRMS	relative residual mean square error [−]
t	time [T]
t^*	time when the transition zone has completely propagated into the column [T]
Δt	time step length [T]
TZ	length of the transition zone [L] between the regions of full and minimum reactivity of ZVI, RR_j

v flow velocity [L T^{-1}]
$V_j^n(t)$ total *(normalised)* deactivated ZVI volume at time t [L]
$V_{\mathrm{ref},j}^n$ *(normalised)* reference ZVI volume [L] deactivated to the minimum reactivity of ZVI; RR_j
$V_{\mathrm{TZ},j}^n$ *(normalised)* deactivated ZVI volume [L] within the transition zone between regions of full and minimum reactivity of ZVI, RR_j
Δx space step length [L]
κ_{ij} fraction of compound i degrading to compound j, i.e. branching ratio [−]
θ_j slope [L^{-1}] that characterises F_j within the transition zone

Acknowledgements

Support for this project is provided by the German Department of Education, Science, Research and Technology (BMBF), Contract No. 02WR0195 and No. 02WR0208. We highly appreciate the suggestions of Prof. Frind and the two anonymous reviewers who helped to improve the paper.

References

Agrawal, A., Ferguson, W.J., Christ, J.A., Bandstra, J.Z., Tratnyek, P.G., 2002. Effects of carbonate species on the kinetics of dechlorination of 1,1,1-trichloroethane by zero-valent iron. Environ. Sci. Technol. 36, 4326–4333.

Arnold, W.A., Roberts, A.L., 2000. Pathways and kinetics of chlorinated ethylene and chlorinated acetylene reaction with Fe(0) particles. Environ. Sci. Technol. 34 (9), 1794–1805.

Bayer, P., 2004. Modelling, economic assessment and optimisation of in-situ groundwater remediation systems. PhD Thesis at the University of Tübingen, Germany, 78 p.

Bayer, P., Finkel, M., 2005. Modeling of sequential groundwater treatment with zero valent iron and granular activated carbon. J. Contam. Hydrol. 78, 129–146.

Bonin, P.M.L., Odziemkowski, M.S., Gillham, R.W., 1998. Electrochemical and Raman spectroscopic studies of the influence of chlorinated solvents on the corrosion behaviour of iron in borate buffer and in simulated groundwater. Corros. Sci. 40, 1391–1409.

Cheng, I.F., Muftikian, R., Fernando, Q., Korte, N., 1997. Reduction of nitrate to ammonia by zero-valent iron. Chemosphere 35 (11), 2689–2695.

Ebert, M., 2004. Elementares Eisen in permeablen reaktiven Barrieren zur in-situ Grundwassersanierung- Kenntnisstand nach zehn Jahren Technologieentwicklung. Habilitation at Christian-Albrechts University of Kiel, Germany. 289 pp.

Ebert, M., Möller, W., Wegner, M., 1999. F+E-Vorhaben reaktive Wand in Rheine-aktuelle Ergebnisse. Altlasten-Spektrum 2 (99), 109–112.

Ebert M., Parbs A., Dahmke A., 2002. Laboruntersuchung zur Dimensionierung eines Fe^0 in-situ Reaktors am Standort Stuttgart/Vaihingen. Institut für Geowissenschaften, Christian-Albrechts-Universität zu Kiel. Project report, unpublished.

Ebert, M., Wegner, M., Parbs, A., Plagentz, V., Köber, R., Dahmke, A., 2003. Prognostizierte und tatsächliche Langzeitstabilität von Fe(0)-Reaktionswänden-Am Beispiel der Reaktionswand am Standort Rheine nach 5-jähriger Betriebszeit. Grundwasser 3, 157–168.

Ebert, M., Köber, R., Parbs, A., Plagentz, V., Schäfer, D., 2006. Assessing degradation rates of chlorinated ethylenes in column experiments with commercial iron materials used in permeable reactive barriers. Environ. Sci. Technol. 40, 2004–2010.

Farrell, J., Kason, M., Melitas, N., Li, T., 2000. Investigation of the long-term performance of zero-valent iron for reductive dechloration of trichloroethylene. Environ. Sci. Technol. 34 (3), 514–521.

Gavaskar, A., Sass, B., Gupta, N., Drescher, E., Yoon, W.S., Sminchak, J., Hicks, J., Condit, W., 2002. Evaluating the Longevity and Hydraulic Performance of Permeable Reactive Barriers at Department of Defense Sites. Battelle Press, Columbus, Ohio.

Gillham, R.W., O'Hannesin, S.F., 1994. Enhanced degradation of halogenated aliphatics by zero-valent iron. Ground Water 32 (6), 958–967.

Gu, B., Phelps, T.J., Liang, L., Dickey, M.J., Roh, Y., Kinsall, B.L., Palumbo, A.V., Jacobs, G.K., 1999. Biogeochemical dynamics in zero-valent iron columns: implications for permeable reactive barriers. Environ. Sci. Technol. 33 (13), 2170–2177.

Hansen, N., Müller, S.D., Koumoustsakos, P., 2003. Reducing the time complexity of the derandomized evolution strategy with covariance matrix adaption (CMA-ES). Evol. Comput. 11 (1), 1–18.

Hatfield, K., Burris, D.R., Wolfe, N.L., 1996. Analytical model for heterogeneous reactions in mixed porous media. J. Environ. Eng. 122, 676–684.

Johnson, T.L., Scherer, M.M., Tratnyek, P.G., 1996. Kinetics of halogenated organic compound degradation by iron metal. Environ. Sci. Technol. 30 (8), 2634–2640.

Klausen, J., Vikesland, P.J., Kohn, T., Burris, D.R., Ball, W.P., Roberts, A.L., 2003. Longevity of granular iron in groundwater treatment processes: solution composition effects on reduction of organohalides and nitroaromatic compounds. Environ. Sci. Technol. 37, 1208–1218.

Köber, R., 2001. Passivating processes in Fe^0 permeable reactive barriers and combinations of Fe^0 and activated carbon or ORC for the remediation of mixed contaminations. PhD Thesis at the University of Kiel, Germany, 112 p.

Kohn, T., Livi, K.J.T., Roberts, A.L., Vikesland, P.J., 2005. Longevity of granular iron in groundwater treatment processes: corrosion product development. Environ. Sci. Technol. 39, 2867–2879.

Kouznetsova, I., 2006. Development and application of a phenomenological modeling concept for simulating the long-term performance of zero-valent iron. PhD Thesis, Eberhard-Karls-University, Tuebingen, Germany.

Li, L., Benson, C.H., Mergener, E.A., 2004. Impact of mineral fouling on hydraulic behavior of permeable reactive barriers. Ground Water 43 (4), 582–596.

Liang, L., West, O.R., Korte, N.E., et al., 1997a. The X-625 Groundwater Treatment Facility: a Field-Scale Test of Trichloroethylene Dechlorinatation Using Iron Fillings for the X-120/X-749 Groundwater Plume. Oak Ridge National Laboratory, TM-13410, Oak Ridge, TN.

Liang, L., Korte, N., Goodlaxson, J.D., Clausen, J., Fernando, Q., Muftikian, R., 1997b. Byproduct formation during the reduction of TCE by zero-valence iron and palladized iron. Ground Water Monit. Remediat. 4, 122–127.

Liedl, R., Finkel, M., Teutsch, G., 1999. In: Weiss, H., Daus, B., Teutsch, G. (Eds.), Modellierung von Abbaureaktionen in *in-situ*-Sanierungreaktoren in UFZ-Bericht "Safira", pp. 84–91.

Matheson, L.J., Tratnyek, P.G., 1994. Reductive dehalogentaion of chlorinated methanes by iron metal. Environ. Sci. Technol. 28, 2045–2053.

Mayer, K.U., Blowes, D.W., Frind, E.O., 2001. Reactive transport modeling of an in situ reactive barrier for the treatment of hexavalent chromium and trichloroethylene in groundwater. Water Resour. Res. 37 (12), 3091–3103.

Miehr, R., Tratnyek, P.G., Bandstra, J.Z., Scherer, M.M., Alowitz, M.J., Bylaska, E.J., 2004. Diversity of contaminant reduction reactions by zerovalent iron: role of the reductate. Environ. Sci. Technol. 38, 139–147.

Möller, W., 1998. Bau einer *"Reaktiven Wand"* als F+E-Vorhaben in Rheine. TerraTech 4.

Morrison, S., 2003. Performance evaluation of a permeable reactive barrier using reaction products as tracers. Environ. Sci. Technol. 37, 2302–2309.

O'Hannesin, S.F., 2004. Plenary Lecture: International Application of PRBs at 1st International Symposium on Permeable Reactive Barriers held at Belfast, UK (March).

O'Hannesin, S.F., Gillham, R.W., 1998. Long-term performance of an in-situ "iron-wall" for remediation of VOCs. Ground Water 36 (1), 164–170.

Okwi, G.J., Thomson, N.R., Gillham, R.W., 2005. The impact of permanganate on the ability of granular iron to degrade trichloroethene. Ground Water Monit. Remediat. 25 (1), 123–128.

Orth, W.S., Gillham, R.W., 1996. Dechlorination of trichloroethene in aqueuos solution using Fe^0. Environ. Sci. Technol. 30 (1), 66–71.

Parbs, A., Ebert, M., Köber, R., Plagentz, V., Schad, H., Dahmke, A., 2003. Einsatz reaktiver Tracer zur Bewertung der Langzeitstabilität und Reaktivität von Fe(0)-Reaktionswänden. Grundwasser 3, 146–156.

Rahman, A., Agrawal, A., 1997. Reduction of nitrate and nitrite by iron metal: implications for groundwater remediation. 213th Am. Chem. Soc. Nat. Meeting, vol. 37 (1), pp. 157–159.

Reynolds, T.J., 2002. An evaluation of the ten-year performance of a permeable reactive barrier including an assessment of the in situ microcosm technique. M.Sc. thesis, Department of Earth Sciences, University of Waterloo, Waterloo, Ontario.

Ritter, K., Odziemkowski, M.S., Simpgraga, R., Gillham, R.W., Irish, D.E., 2003. An in situ study of the effect of nitrate on the reduction of trichloroethylene by granular iron. J. Contam. Hydrol. 65, 121–136.

Schäfer, D., Köber, R., Dahmke, A.J., 2003. Competing TCE- and *cis*-DCE-degradation kinetics by zero-valent iron — experimental results and numerical simulation. J. Contam. Hydrol. 65, 183–202.

Scherer, M.M., Richter, S., Valentine, R.L., Alvarez, P.J.J., 2000. Chemistry and microbiology of permeable reactive barriers for in situ groundwater cleanup. Crit. Rev. Environ. Sci. Technol. 30 (3), 363–411.

Schlicker, O., Ebert, M., Fruth, M., Weidner, M., Wüst, W., Dahmke, A., 2000. Degradation of TCE with iron: the role of competeing chromate and nitrate reduction. Ground Water 38 (3), 403–409.

Sinatar, D.P., Schreier, C.G., Reinhard, M., 1995. Transformation of the pesticide 1,2-dibrome-3-chloropropane (DBCP) and nitrate by iron powder and by H2/Pd/Al2O3. 209th Am. Chem. Soc. Nat. Meeting, Div. Envir. Chem., vol. 35, pp. 745–746.

Su, C., Puls, R.W., 1999. Kinetics of trichloroethene Reduction by zerovalent iron and tin: pretreatment effect, apparent activation energy, and intermediate products. Environ. Sci. Technol. 33 (1), 163–168.

Tratnyek, P.G., Johnson, T.L., Scherer, M.M., Eykholt, G.R., 1997. Remediating ground water with zero-valent metals: chemical considerations in barrier design. Ground Water Monit. Remediat. 108–114.

Tratnyek, P.G., Scherer, M.M., Deng, B., Hu, S., 2001. Effects of natural organic matter, anthropogenic surfactants, and model quinones on the reduction of contaminants by zero-valent iron. Water Res. 35 (18), 4435–4443.

Vikesland, P.J., Klausen, J., Zimmermann, H., Roberts, A.L., Ball, W.P., 2003. Longevity of granular iron in groundwater treatment processes: changes in solute transport properties over time. J. Contam. Hydrol. 64, 3–33.

Vogan, J.L., Gillham, R.W., O'Hannesin, S.F., Matulewicz, W.H., Rhodes, J.E., 1995. Site specific degradation of VOCs in groundwater using zero valent. Natl. Meet. - Am. Chem. Soc., Div. Environ. Chem. 35, 792–795.

Wang, J., Farrell, J., 2003. Investigating the role of atomic hydrogen on chloroethene reactions with iron using Tafel analysis and electrocehemical impedence spectroscopy. Environ. Sci. Technol. 37, 3891–3896.

Wilkin, R.T., Puls, R.W., 2003. Capstone report on the application, monitoring, and performance of permeable reactive barriers for groundwater remediation, vol. 1, EPA/600/R-03/045.

Wilkin, R.T., Puls, R.W., Sewell, G.W., 2002. Long-term performance of permeable reactive barriers using zero-valent iron: an evaluation at two sites. Environ. Research Brief, EPA/600/S-02/001.

Wilkin, R.T., Puls, R.W., Sewell, G.W., 2003. Long-term performance of permeable reactive barriers using zero-valent iron: geochemical and microbiological effects. Ground Water 41 (4), 493–503.

Wüst, W.F., Köber, R., Schlicker, O., Dahmke, A., 1999. Combined zero-and first-order kinetic model of the degradation of TCE and *cis*-DCE with commercial iron. Environ. Sci. Technol. 33 (23), 4304–4309.

Yabusaki, S., Cantrell, K., Sass, B., Steefel, C., 2001. Multicomponent reactive transport in an in situ zero-valent iron cell. Environ. Sci. Technol. 35 (7), 1493–1503.

Yamane, C.L., Warner, C.D., Gallinatti, J.D., Szerdy, F.S., Delfino, T.A., 1995. Natl. Meet. - Am. Chem. Soc., Div. Environ. Chem. 35, 800–804.

Zhang, Y., Gillham, R., 2005. Effects of gas generation and precipitates on performance of Fe^0 PRBs. Ground Water 43 (1), 113–121.